

Topology of the $O(3)$ non-linear sigma model under the gradient flow

Stuart Thomas^{a,*} and Christopher Monahan^{a,b}

^a*Department of Physics, William & Mary,
300 Ukrop Way, Williamsburg, VA, USA*

^b*Thomas Jefferson National Accelerator Facility,
12000 Jefferson Avenue, Newport News, VA, USA*

E-mail: snthomas01@email.wm.edu, cjmonahan@wm.edu

The $O(3)$ non-linear sigma model (NLSM) is a prototypical field theory for QCD and ferromagnetism, featuring topological qualities. Though the topological susceptibility χ_t should vanish in physical theories, lattice simulations of the NLSM find that χ_t diverges in the continuum limit. We study the effect of the gradient flow on this quantity using a Markov Chain Monte Carlo method, finding that a logarithmic divergence persists. This result supports a previous study and indicates that either the definition of topological charge is problematic or the NLSM has no well-defined continuum limit. We also introduce a θ -term and analyze the topological charge as a function of θ under the gradient flow.

*The 38th International Symposium on Lattice Field Theory, LATTICE2021 26th-30th July, 2021
Zoom/Gather@Massachusetts Institute of Technology*

*Speaker

1. Introduction

Spin models provide a framework for understanding the physics of strongly-coupled systems, from solid state and condensed matter systems to nuclear and particle physics. The non-linear sigma model (NLSM), in particular, has provided a rich arena in which to study nonperturbative effects. In solid-state systems, this model describes Heisenberg ferromagnets [1] and in nuclear physics, it acts as a prototype for quantum chromodynamics (QCD), the gauge theory of the strong nuclear force. In general, the NLSM shares key features with non-Abelian gauge theories such as QCD, including a mass gap and asymptotic freedom [2], and has proved a useful model for exploring the effect of these properties in a simpler system.

We consider the $O(3)$ NLSM in 1+1 dimensions (one dimension of space, one dimension of time). This theory exhibits topological properties, such as *instantons*, or classical field solutions at local minima of the action in Euclidean space. These topologically protected solutions cannot evolve into the vacuum state via local fluctuations. This property has become critically important to quantum field theories in cosmology and high energy physics [3]. *CJM: Can we provide a more explicit example(s) here? Statement is very vague at the moment.* Additionally, topological stability may become a key tool for fault-tolerant quantum computers [4]. In these devices, topology protects the delicate quantum states necessary for information processing.

The protection of topological instantons in the 1+1 $O(3)$ NLSM relies on a vanishing topological susceptibility. However, the convergence of this quantity is still unknown. [5] While the some analytical arguments argue the topological susceptibility should approach zero in the continuum limit, numerical results on the lattice predict infinities [6]. In an attempt to shed light on this contradiction, we apply the gradient flow, a local smearing of operators which preserves gauge invariance. In quantum chromodynamics, this technique has corroborated a previous analytical result [7] by removing ultraviolet divergences on the lattice [8]. This success has motivated the gradient flow to calculate the topological susceptibility in the 1+1 $O(3)$ NLSM. Despite this intuition, recent studies demonstrate that the observable still diverges in the continuum limit [5].

We also study a second perspective on the topological susceptibility arising from the introduction of a θ -term into the field Lagrangian. This term drives the vacuum state into a topological phase [9]. Differentiating the field's partition function with respect to θ yields a value proportional to the topological susceptibility. The effect of nonzero θ on the theory therefore should reflect the divergence in the continuum limit. In this work we verify the divergence of the topological susceptibility and develop a clearer picture of how the θ -term affects the topology of the 1+1 $O(3)$ NLSM.

To numerically study the topological qualities of the NLSM, we first implement a Markov chain Monte Carlo simulation using Metropolis and Wolff cluster [10] algorithms. Since the gradient flow has no exact solution in the NLSM we implement a numerical solution using a fourth-order Runge-Kutta approximation with automatic step sizing. By applying the gradient flow to every configuration in the sample, we can measure its effect on the topological charge and susceptibility.

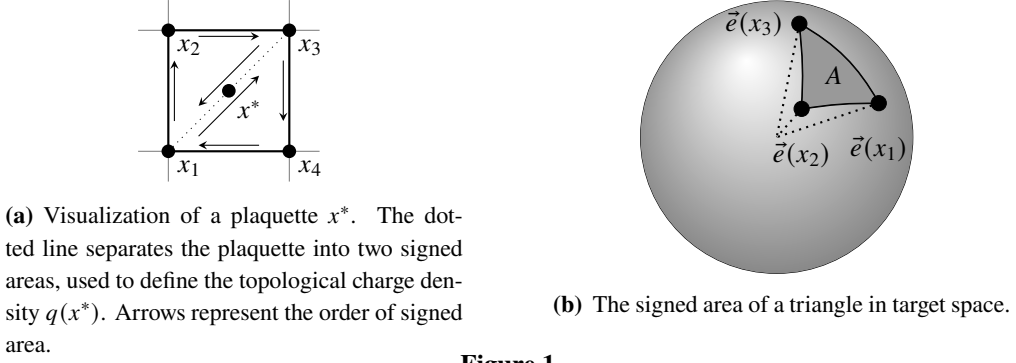


Figure 1

2. The non-linear sigma model

CJM: [In Euclidean space it does not really make sense to distinguish time and space, unless we start in Minkowski spacetime and then Wick rotate.]

SNT: I think I resolved this

We study the $O(3)$ NLSM in two dimensions, defined by the Euclidean action

$$S_E = \frac{\beta}{2} \int d^2x \sum_{i=1}^2 (\partial_i \vec{e})^2,$$

where \vec{e} is 3-component real vector constrained by $|\vec{e}| = 1$ and β is the inverse coupling constant. Following [6], we define the topological charge density, $q(x^*)$, for each plaquette x^* such that the total topological charge is

$$Q = \sum_{x^*} q(x^*), \quad (1)$$

where

$$q(x^*) = \frac{1}{4\pi} \left[A(\vec{e}(x_1), \vec{e}(x_2), \vec{e}(x_3)) + A(\vec{e}(x_1), \vec{e}(x_3), \vec{e}(x_4)) \right]. \quad (2)$$

Here, A is the signed area of the triangle in target space, which we represent in the left-hand figure of Fig. 1b. This value is defined if $A \neq 0, 2\pi$, or in other words, as long as the three points on the sphere are distinct and do not form a hemisphere. In numerical calculations, these points can be ignored. Therefore, we impose that the signed area is defined on the smallest spherical triangle, or $-2\pi < A < 2\pi$.

We define the topological susceptibility χ_t

$$\chi_t \equiv \frac{1}{L^2} (\langle Q^2 \rangle - \langle Q \rangle^2). \quad (3)$$

In the trivial case, $\langle Q \rangle$ is equal to 0 and on this lattice, this becomes

$$\chi_t = \frac{1}{L^2} \sum_{x^*} \langle q(x^*) q(0) \rangle, \quad (4)$$

where we have assumed periodic boundary conditions. In the continuum limit, the topological susceptibility diverges owing solely to the $x^* = 0$ term [5], a divergence that exists in QCD as well [8].

Additionally, we can generalize the NLSM to have a nonzero vacuum expectation value for the topological charge, manifested by the addition of a “ θ -term”:

$$S[\vec{e}] \rightarrow S[\vec{e}] - i\theta Q[\vec{e}].$$

defining the “nontrivial” NLSM. We find that the topological susceptibility in the trivial case depends on the charge in the nontrivial model:

$$\chi_t \propto \left. \frac{d \text{Im}\langle Q \rangle}{d\theta} \right|_{\theta=0} \quad (5)$$

3. Gradient flow

To remove this ultraviolet divergence, we adopt a technique known as “smearing”, a local averaging of the field [11]. Specifically, we use a technique known as the gradient flow [12] which introduces a new half-dimension¹ called “flow time”. The flow time τ parameterizes the smearing such that an evolution in flow time corresponds to suppressing ultraviolet divergences, pushing field configurations toward classical minima of the action.

We can choose any flow time equation that drives the field towards a classical minimum. Following [5], we can define the gradient flow for the NLSM via the differential equation

$$\partial_\tau \vec{e}(\tau, x) = \left(1 - \vec{e}(\tau, x) \vec{e}(\tau, x)^T \right) \partial^2 \vec{e}(\tau, x). \quad (6)$$

We solve this equation numerically using the boundary condition $\vec{e}(\tau = 0, x) = \vec{e}(x)$, a process described in Sec. 4.

4. Numerical implementation

We implement a numerical Monte Carlo method to study the NLSM in two dimensions using the discretized action

$$S_{\text{lat}}[\vec{e}] = \sum_i \left[2 - \sum_{\mu=0}^2 \vec{e}(x + a\hat{\mu}) \cdot \vec{e}(x) \right] \quad (7)$$

where a is a lattice constant and $\hat{\mu}$ are the Euclidean unit vectors. We generate configurations using the Metropolis [SNT: Does this need to be cited?](#) and Wolff cluster [10] algorithms.

We thermalize the configurations with 1000 sweeps, with a cluster update every five sweeps, and illustrate a sample Markov chain in Fig. 2, where we plot the action as a function of Metropolis sweeps. We use Wolff’s automatic windowing procedure [13] to estimate the autocorrelation times for various observables, such as the magnetic susceptibility χ_m . We measure observables every 50 sweeps for each simulation.

We apply the gradient flow equation

$$\partial_\tau \vec{e}(\tau, x) = \left(1 - \vec{e}(\tau, x) \vec{e}(\tau, x)^T \right) \partial^2 \vec{e}(\tau, x), \quad (8)$$

¹The term “half-dimension” indicates that the flow time is exclusively positive.

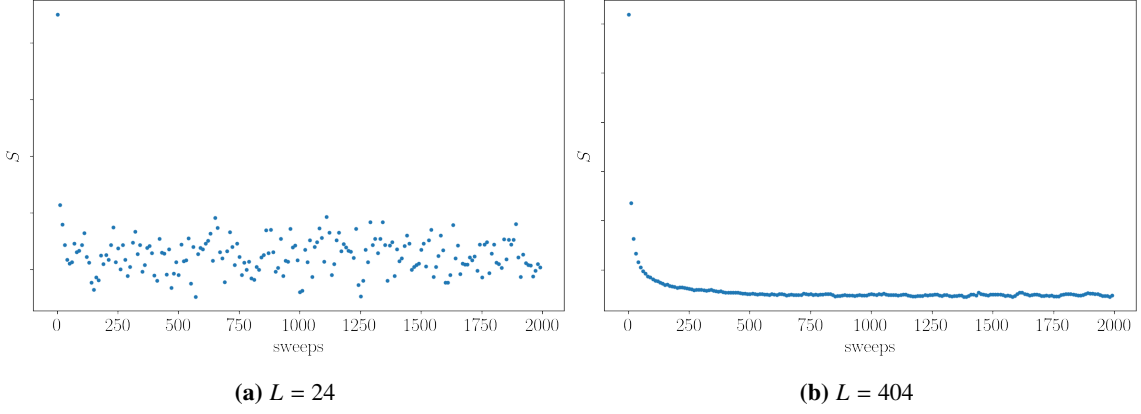


Figure 2: Plots of the action as a function of Monte Carlo time, starting with a random NLSM lattice.

replacing the continuous Laplacian operator ∂^2 with a discrete analogue

$$\partial^2 \vec{e}(\tau, x) = \vec{e}(\tau, x + a\hat{t}) + \vec{e}(\tau, x - a\hat{t}) + \vec{e}(\tau, x + a\hat{x}) + \vec{e}(\tau, x - a\hat{x}) - 4\vec{e}(\tau, x).$$

We numerically solve the ordinary differential equation in Eq. ?? using a fourth-order Runge-Kutta approximation. To increase the efficiency of this algorithm, we implement the step-doubling algorithm to adaptively adjust the step size. If the error of a Runge-Kutta step is greater than the tolerance, the same step is repeated with half the step size. Alternatively, if the error is less than half of the tolerance, the step size is doubled for the next calculation. Finally, if the step size is greater than the distance to the next measurement, that distance is used as the step size, using the normal value afterwards. Otherwise, the algorithm proceeds with the consistent step size.

To calculate the error, we compare one lattice \vec{e}_1 produced using a step of size $2h$ with another lattice \vec{e}_2 produced via two steps of size h . The error Δ can be estimated up to the fifth order of h as [14]

$$\Delta = \frac{1}{15} \sqrt{\sum_x |\vec{e}_2(x) - \vec{e}_1(x)|^2} \quad (9)$$

The tolerance used in this work is $\Delta_{max} = 0.01$.

5. Results

In order to confirm the accuracy of the model, we compare results with existing literature. We first consider the results of Berg & Lüscher [6], specifically the internal energy and magnetic susceptibility. Following [6], we approximate the internal energy in the strong ($\beta < 1$) and weak ($\beta > 2$) regimes as

$$E \approx \begin{cases} 4 - 4y - 8y^3 - \frac{48}{5}y^5 & \beta < 1 \\ \frac{2}{\beta} + \frac{4}{\beta^2} + 0.156\frac{1}{\beta^3} & \beta > 2 \end{cases} \quad (10)$$

where

$$y = \coth\beta - \frac{1}{\beta}. \quad (11)$$

We compare this analytical result and simulated values of χ_m with the Monte Carlo simulation in Fig. 3. These two charts show a high degree of agreement with the current literature however there

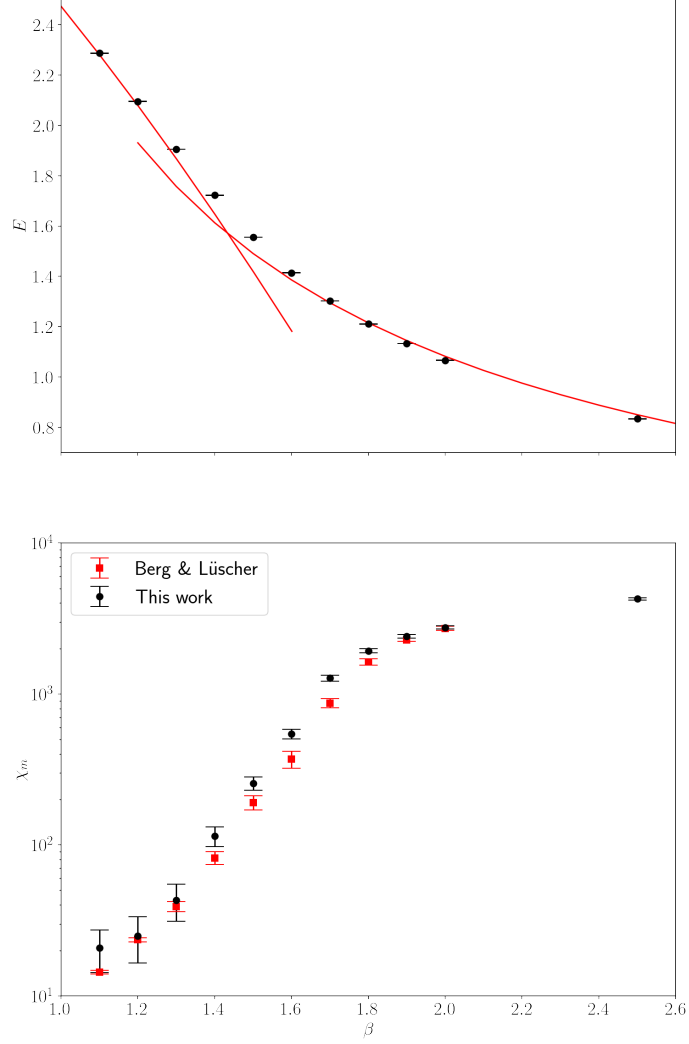


Figure 3: Comparison with [6]. First panel: internal energy compared with analytic energy (Eq. 10). Second panel: magnetic susceptibility compared with literature values.

is a slight discrepancy, perhaps arising from different Monte Carlo methods.

We also seek to confirm the results from Bietenholz et al. [5]. Specifically, we show the topological susceptibility χ_t diverges in the continuum limit even at finite flow time. Since χ_t is in units of inverse distance squared, we multiply by ξ_2^2 , the square of the second moment correlation length, to achieve a scale-invariant value $\chi_t \xi_2^2$. Additionally, we use a parameter t_0 to scale the flow time such that $t_0 \sim L^2$. In our Monte Carlo simulation, we utilize the same values as [5] for ξ_2 , β and t_0 .

To begin the comparison, we plot $\chi_t \xi_2^2$ as a function of flow time τ , shown in Fig. 4. We find that the flow time effectively decreases the topological susceptibility by dampening high-momentum modes. To analyze the divergence of χ_t in the continuum limit, we plot $\chi_t \xi_2^2$ as a function of lattice size L . We perform this simulation at flow times $\tau = 0$ and $\tau = 5t_0$ (Fig. 5). We fit the data with

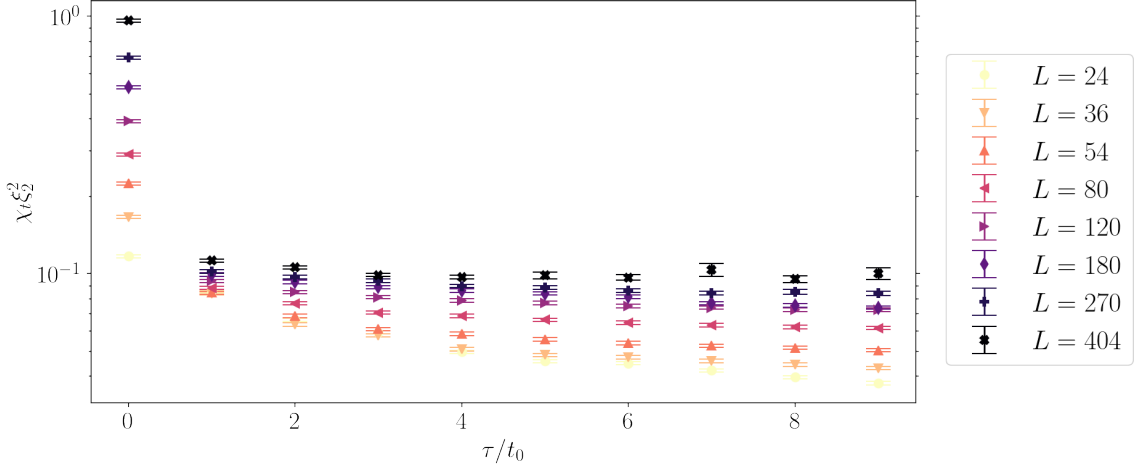


Figure 4: $\chi_t L^2$ as a function of flow time τ . Simulation run with 10,000 measurements every 50 sweeps, 1,000 sweep thermalization.

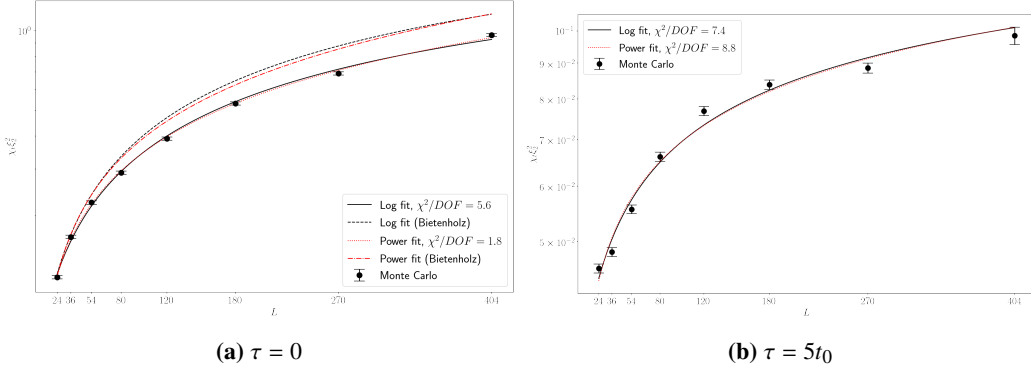


Figure 5: $\chi_t \xi_2^2$ as a function of L . We fit the data with both a logarithmic and power fit. Simulation run with 10,000 measurements, once every 50 sweeps, 1,000 sweep thermalization. In the $\tau = 0$ case, we have compared our result with the curve fit found in [5].

two options: a log fit

$$\chi_t \xi_2^2 = a \log(bL + c) \quad (12)$$

and a power law fit

$$\chi_t \xi_2^2 = aL^b + c. \quad (13)$$

We calculate the parameters to these functions using the `curve_fit` tool in the `scipy` Python package [15]. When $\tau = 5t_0$, the data fits these functions with χ^2/DOF of 7.4 and 8.8 respectively, indicating errors were underestimated. Both of these functions diverge as $L \rightarrow \infty$, indicating that the topological susceptibility also diverges in the continuum limit. Though there is a clear difference between the quantitative fit from [5] and the fit calculated in this work, both demonstrate divergent behavior. This result supports the inherent divergence of χ_t in the continuum limit.

5.1 Topological Charge when $\theta \neq 0$

Following the method explained in Sec. ??, we calculate the imaginary part of $\langle Q \rangle$ for arbitrary θ . We perform this calculation for three values of the flow time τ , shown in Fig 6. These plots

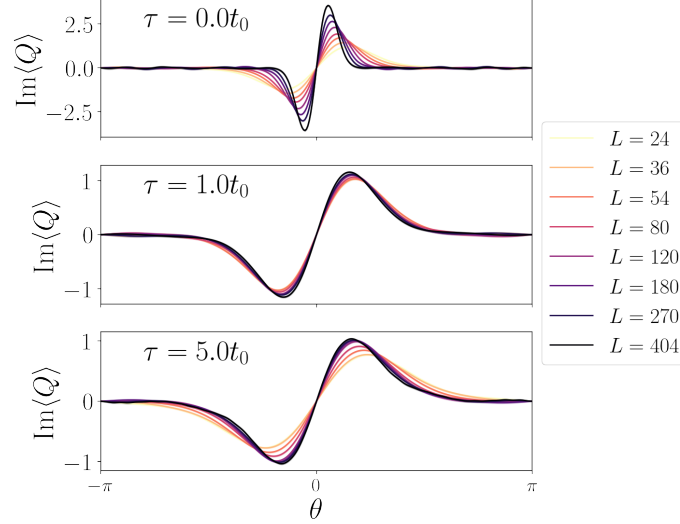


Figure 6: Imaginary part of $\langle Q \rangle$ as a function of θ . Simulation run with 10,000 measurements, measurements very 50 sweeps, 1,000 sweep thermalization. Note the different scaling of the y-axis.

demonstrate the divergence of the continuum limit in the $\tau = 0$ and the flowed regimes. In the $\tau = 0$ case, the slope increases sharply, reflecting the rapid divergence of χ_t . However in the flowed regime, this divergence is much slower, reflecting the decreased values of χ_t shown in Fig. 4.

Berg & Lüscher [6] originally illuminated this discrepancy between the renormalization group hypothesis (that $\chi_t \rightarrow 0$) and the numerical results, providing three possible causes:

1. The definition of the topological charge does not scale to the continuum.
2. There are ultraviolet divergences.
3. There is no reasonable continuum limit.

Since the gradient flow suppresses ultraviolet fluctuations, the persistence of a divergent topological susceptibility under the gradient flow undermines the second option, thereby supporting the other two.

References

- [1] C. Callan, D. Friedan, E. Martinec and M. Perry, *Strings in background fields*, .
- [2] A. Polyakov, *Interaction of goldstone particles in two dimensions. Applications to ferromagnets and massive Yang-Mills fields*, .
- [3] P. Goddard and P. Mansfield, *Topological structures in field theories*, .

- [4] A.Y. Kitaev, *Quantum computations: Algorithms and error correction*, .
- [5] W. Bietenholz, P. de Forcrand, U. Gerber, H. Mejía-Díaz and I.O. Sandoval, *Topological Susceptibility of the 2d $O(3)$ Model under Gradient Flow*, [1808.08129](#).
- [6] B. Berg and M. Lüscher, *Definition and statistical distributions of a topological number in the lattice $O(3)$ σ -model*, .
- [7] L. Giusti, G. Rossi and M. Testa, *Topological susceptibility in full QCD with Ginsparg–Wilson fermions*, .
- [8] M. Bruno, S. Schaefer, R. Sommer and ALPHA Collaboration, *Topological susceptibility and the sampling of field space in $N_f = 2$ lattice QCD simulations*, .
- [9] B. Alles Salom and A. Papa, *Numerical Study of the mass spectrum in the 2D $O(3)$ sigma model with a theta term*, in *Proceedings of The XXV International Symposium on Lattice Field Theory — PoS(LATTICE 2007)*, p. 287, Sissa Medialab, [DOI](#).
- [10] U. Wolff, *Collective monte carlo updating for spin systems*, .
- [11] S. Solbrig, F. Bruckmann, C. Gattringer, E.-M. Ilgenfritz, M. Muller-Preussker and A. Schafer, *Quantitative comparison of filtering methods in lattice QCD*, .
- [12] C. Monahan and K. Orginos, *Locally smeared operator product expansions in scalar field theory*, .
- [13] U. Wolff, *Monte Carlo errors with less errors*, [hep-lat/0306017](#).
- [14] W.T. Vetterling, W.H. Press, S.A. Teukolsky and B.P. Flannery, *Numerical Recipes: Example Book C*, Cambridge University Press.
- [15] P. Virtanen, R. Gommers, T.E. Oliphant, M. Haberland, T. Reddy, D. Cournapeau et al., *SciPy 1.0: Fundamental algorithms for scientific computing in python*, .